Mutations in *CRADD* Result in Reduced Caspase-2-Mediated Neuronal Apoptosis and Cause Megalencephaly with a Rare Lissencephaly Variant

Nataliya Di Donato,[1,2,17,*] Ying Y. Jean,[3] A. Murat Maga,[4,5] Briana D. Krewson,[6] Alison B. Shupp,[6] Maria I. Avrutsky,[3] Achira Roy,[2] Sarah Collins,[2] Carissa Olds,[2] Rebecca A. Willert,[6] Agnieszka M. Czaja,[6] Rachel Johnson,[6] Jessi A. Stover,[6] Steven Gottlieb,[7] Deborah Bartholdi,[8] Anita Rauch,[9] Amy Goldstein,[10] Victoria Boyd-Kyle,[6] Kimberly A. Aldinger,[2] Ghayda M. Mirzaa,[2,11] Anke Nissen,[12] Karlla W. Brigatti,[6,13] Erik G. Puffenberger,[6,13] Kathleen J. Millen,[2] Kevin A. Strauss,[6,13,14] William B. Dobyns,[2,11,15,17] Carol M. Troy,[3,16,17] and Robert N. Jinks[6,17,*]

Lissencephaly is a malformation of cortical development typically caused by deficient neuronal migration resulting in cortical thickening and reduced gyration. Here we describe a "thin" lissencephaly (TLIS) variant characterized by megalencephaly, frontal predominant pachygyria, intellectual disability, and seizures. Trio-based whole-exome sequencing and targeted re-sequencing identified recessive mutations of *CRADD* in six individuals with TLIS from four unrelated families of diverse ethnic backgrounds. CRADD (also known as RAIDD) is a death-domain-containing adaptor protein that oligomerizes with PIDD and caspase-2 to initiate apoptosis. TLIS variants cluster in the CRADD death domain, a platform for interaction with other death-domain-containing proteins including PIDD. Although caspase-2 is expressed in the developing mammalian brain, little is known about its role in cortical development. CRADD/caspase-2 signaling is implicated in neurotrophic factor withdrawal- and amyloid-β-induced dendritic spine collapse and neuronal apoptosis, suggesting a role in cortical sculpting and plasticity. TLIS-associated CRADD variants do not disrupt interactions with caspase-2 or PIDD in co-immunoprecipitation assays, but still abolish CRADD's ability to activate caspase-2, resulting in reduced neuronal apoptosis in vitro. Homozygous *Cradd* knockout mice display megalencephaly and seizures without obvious defects in cortical lamination, supporting a role for CRADD/caspase-2 signaling in mammalian brain development. Megalencephaly and lissencephaly associated with defective programmed cell death from loss of CRADD function in humans implicate reduced apoptosis as an important pathophysiological mechanism of cortical malformation. Our data suggest that CRADD/caspase-2 signaling is critical for normal gyration of the developing human neocortex and for normal cognitive ability.

Introduction

Folding of the human cerebral cortex into its complex pattern of gyri and sulci and the precise layering of neurons within the cortex (cortical lamination) depend upon a finely tuned program of neuronal proliferation, migration, connectivity, and pruning.[1–5] Lissencephaly is a cortical malformation characterized by abnormally broad or absent gyri with unusually thick cortex (10–20 mm, normal range 1–4.5 mm[6]) that is classically caused by deficient neuronal migration.[7–10] From review of phenotypes in more than 1,400 subjects with lissencephaly, we identified a relatively mild variant characterized by anterior-predominant pachygyria with shallow and unusually wide sulci, mildly thick cortex (5–7 mm) in at least the frontal regions, and no non-cortical malforma-

tions in 13 families, a pattern we refer to as "thin" lissencephaly (TLIS). Several families had multiple affected siblings, indicative of autosomal-recessive inheritance. Similar phenotypes have been reported a few times, but with no underlying cause identified (MIM: 610279).[11–14] We performed trio-based whole-exome sequencing in two families with TLIS and detected a homozygous mutation of *CRADD* (GenBank: NM_003805.3; c.382G>C [p.Gly128Arg] [MIM: 603454]) in two siblings from a Mennonite family. Targeted re-sequencing of an additional 18 unrelated individuals with TLIS identified two other homozygous missense mutations in *CRADD* (c.508C>T [p.Arg170Cys] and c.509G>A [p.Arg170His]) in families of Turkish and Finnish ancestry, respectively, and a fourth missense change (c.491T>G [p.Phe164Cys]) in *trans* with a 3.07 Mb deletion of chromosome 12q22

[1]Institute for Clinical Genetics, Faculty of Medicine Carl Gustav Carus, TU Dresden, 01307 Dresden, Germany; [2]Center for Integrative Brain Research, Seattle Children's Research Institute, Seattle, WA 98105, USA; [3]Department of Pathology and Cell Biology, Columbia University Medical Center, New York, NY 10032, USA; [4]Center for Developmental Biology and Regenerative Medicine, Seattle Children's Research Institute, Seattle, WA 98105, USA; [5]Division of Craniofacial Medicine, Department of Pediatrics, University of Washington, Seattle, WA 98105, USA; [6]Department of Biology, Biological Foundations of Behavior Program, Franklin & Marshall College, Lancaster, PA 17604, USA; [7]Division of Pediatric Neurology, Nemours Alfred I. DuPont Hospital for Children, Wilmington, DE 19803, USA; [8]Department of Human Genetics, Inselspital, 3010 Bern, Switzerland; [9]Institute of Medical Genetics, University of Zurich, 8952 Schlieren, Switzerland; [10]Department of Pediatrics, School of Medicine, University of Pittsburgh, Children's Hospital of Pittsburgh of UPMC, Pittsburgh, PA 15224, USA; [11]Department of Pediatrics, University of Washington, Seattle, WA 98195, USA; [12]Medical Genetics Center, 80335 Munich, Germany; [13]Clinic for Special Children, Strasburg, PA 17579, USA; [14]Lancaster General Hospital, Lancaster, PA 17602, USA; [15]Department of Neurology, University of Washington, Seattle, WA 98195, USA; [16]The Taub Institute for Research on Alzheimer Disease and the Aging Brain, Columbia University Medical Center; Department of Neurology, Columbia University Medical Center, New York, NY 10032, USA
[17]These authors contributed equally to this work
*Correspondence: nataliya.didonato@uniklinikum-dresden.de (N.D.D.), rjinks@fandm.edu (R.N.J.)
http://dx.doi.org/10.1016/j.ajhg.2016.09.010.

that includes *CRADD* in an affected child of a fourth family.

CRADD encodes caspase-recruitment-domain and death domain (DD)-containing protein (also known as RAIDD, receptor-interacting protein-associated ICH-1/CED-3 homologous protein with a death domain), which is required for activation of caspase-2-mediated apoptosis.[15,16] In general, CRADD serves as an adaptor between PIDD (p53-induced death domain-containing protein 1, *PIDD1* [MIM: 605247]) and caspase-2 (*CASP2* [MIM: 600639]) during formation of the apoptosis-promoting PIDDosome.[15–18] Phosphorylation of PIDD by signaling associated with cellular or genotoxic stress stimulates binding of the PIDD-DD to the CRADD-DD, which in turn allows the caspase recruitment domain (CARD) of CRADD to bind and activate caspase-2.[15–20] Dendritic spine collapse and neuronal apoptosis induced by neurotrophic factor withdrawal or amyloid-β aggregation can be initiated by CRADD/caspase-2 signaling in the absence of PIDD, suggesting that formation of the PIDDosome may not be required for caspase-2-driven synaptic remodeling and neuronal apoptosis.[21,22]

The caspases are intracellular proteases that maintain homeostasis through regulation of inflammation (caspase-1, -4, -5, -12) and apoptosis (caspase-2, -3, -6, -7, -8, -9).[4] During mammalian brain development, caspase-3 (*CASP3* [MIM: 600636]) is the primary executioner of synaptic and neuronal pruning and is activated by the mitochondrial (intrinsic) apoptotic cascade through APAF1 (apoptotic protease-activating factor 1 [MIM: 602233])/caspase-9 (*CASP9* [MIM: 602234]) activation.[2,4,23,24] Although caspase-2 is expressed in neurons in the embryonic and adult mammalian brain,[25–28] its role in brain development has been elusive.[4]

Here we show that the human CRADD variants associated with TLIS abrogate CRADD's ability to activate caspase-2 and drive neuronal apoptosis. The megalencephaly, lissencephaly variant, and intellectual disability associated with loss of CRADD/caspase-2-mediated apoptosis imply a role for CRADD/caspase-2 signaling in development of the human cerebral cortex.

Subjects and Methods

Research Subjects

W.B.D. has ascertained ~1,400 children with lissencephaly or subcortical band heterotopia over the last 30 years. Clinical information and results of genetic testing were obtained from medical records submitted together with MRI scans by referring physicians or parents of the subjects. Genetic testing included results of chromosome analysis, fluorescence in situ hybridization for deletion 17p13.3 (MIM: 247200), chromosome microarrays, MLPA for *LIS1* (*PAFAH1B1* [MIM: 601545]) and *DCX* (MIM: 300121), Sanger sequencing of single genes (*LIS1*, *DCX*, *ARX* [MIM: 300382], *TUBA1A* [MIM: 602529], *TUBB2B* [MIM: 612850], *RELN* [MIM: 600514], *VLDLR* [MIM: 192977], *ACTB* [MIM: 102630], and *ACTG1* [MIM: 102560]), targeted gene panels, and whole-exome

sequencing. We re-reviewed scans of 188 subjects ascertained between 2009 and 2015, when high-resolution scans were available for most individuals. All were reviewed with particular attention to the severity and gradient of the gyral malformation, cortical thickness, and presence of associated brain malformations.

Thin undulating LIS with normal cerebellum (TLIS) was seen in 9 of 188 subjects (5%). We also searched W.B.D.'s large research database for subjects with frontal pachygyria and normal cerebellum and corpus callosum and identified 12 additional individuals with the specific TLIS pattern. Several had large or relatively large occipitofrontal circumference (OFC), which we subdivide into true (OFC > 3 SD above the mean), mild (OFC 2–3 SD above the mean), and relative (OFC more than 2 SD greater than height) megalencephaly.[29]

Institutional review boards at The University of Chicago and Seattle Children's Hospital approved this study. Seven members of an additional Mennonite family carrying *CRADD* c.382G>C and receiving medical care at the Clinic for Special Children (Strasburg, PA) were added to the study (see Results). Their participation was approved by the Institutional Review Board at Lancaster General Hospital. Informed consent signed by the parents or legal guardians was obtained for all participating individuals.

Whole-Exome Sequencing

Exome capture and sequencing were done using Agilent SureSelect Human All Exon V5 enrichment and Illumina HiSeq 2500 sequencing (paired-end 2 × 100 nt). The sequencing data were processed using CLC Biomedical Genomics Workbench (QIAGEN) including read alignment to UCSC Genome Browser hg19, variant calling (SNPs and indels), annotation, and filtering against three public databases (ExAC, dbSNP, and 1000 Genomes Project). For each sample, the average coverage through the exome was 80-fold and more than 90% of the exome was covered at least 20-fold. We focused on protein-altering and splice-site variants absent in databases or present with allele frequencies below 0.01. We filtered variants to systematically identify homozygous variants that were heterozygous in both parents, compound-heterozygous variants inherited from one parent, as well as de novo variants.

Targeted Panel Sequencing with Single-Molecule Molecular Inversion Probe

Using an established MIPGEN pipeline,[30] we designed a pool of 673 single-molecule molecular inversion probes (smMIP) targeting the coding regions of 16 known LIS-associated genes—*ACTB*, *ACTG1*, *ARX*, *DCX*, *DYNC1H1* (MIM: 600112), *KIF2A* (MIM: 602591), *KIF5C* (MIM: 604593), *LIS1*, *RELN*, *TUBA1A*, *TUBA8* (MIM: 605742), *TUBB* (MIM: 191130), *TUBB2B* (MIM: 612850), *TUBB3* (MIM: 602661), *TUBG1* (MIM: 191135), and *VLDLR*—and our candidate gene, *CRADD*. In total, smMIPs were tiled across 47,975 bp of coding sequence. Capture reactions (100 ng) were performed in parallel using previously published protocols.[30,31] Massively parallel sequencing was done on the Illumina HiSeq and MiSeq platforms. The average collapsed coverage (number of single-molecule consensus sequences or "smc-reads")[31] across all samples was 21.

Cradd Knockout Mice

Cradd$^{-/-}$ mice on a C57BL/6 background were obtained from the Jackson Laboratories with permission from Prof. Tak Mak (University of Toronto).[17] Wild-type (WT) C57BL/6 mice were also obtained from the Jackson Laboratories and all mice were

maintained under pathogen-free conditions. All animal experiments were approved by the Institutional Animal Care and Use Committees (IACUC) of Franklin & Marshall College and Columbia University Medical Center.

Whole-Animal Perfusion Fixation

Transcardial perfusion fixation was used to prepare mouse heads/brains (as described elsewhere[32]) for micro-CT and histological analyses. In brief, mice were anesthetized by intraperitoneal (i.p.) injection of ketamine/xylazine mixture (up to 80 mg/kg body weight ketamine and 10 mg/kg body weight xylazine). When a surgical plane of anesthesia was achieved, the heart was exposed, a 23G cannula inserted into the ascending aorta via the left ventricle, and a perfusate exit hole placed in the right atrium. The circulation was slowly flushed with 20–30 mL of phosphate buffered saline (PBS; pH 7.4) followed by perfusion of 30–40 mL of 0.22 μm sterile-filtered, freshly prepared 4% paraformaldehyde in PBS. Upon complete blanching of the liver and mesentery, mice were decapitated and intact skulls and brains were postfixed overnight in 4% paraformaldehyde in PBS at 4°C.

Cortical/Brain Histology

Dissected brains were infiltrated with 30% sucrose in PBS, embedded in optimum cutting temperature (OCT) compound, and sectioned at 20 μm on a cryostat. Every 10th section was placed on a slide and stained in 0.1% cresyl violet solution for 10 min, rinsed quickly in PBS, dehydrated in 95% ethanol, and left in xylene before being coverslipped with Permount (Fisher Scientific). Brightfield images were taken using a Leica MZFLIII microscope with a Leica DFC425 camera and LAS V3.8 software.

Volumetric Mouse Skull CT

A total of 17 skulls were imaged at the Small Animal Tomographic Analysis Lab at Seattle Children's Research Institute using a Skyscan 1076C microtomograph (Bruker) with settings optimized for mouse skulls (voltage, 55 kV; current, 180 μA; 0.5 mm Al filter; 100 ms exposure; 0.6° rotation steps; three frames averaged per rotation; 360° degree full rotation). Scan duration was approximately 10 min per sample. 600 shadow images were acquired per specimen, which were reconstructed as image stacks at 34.42-micron resolution using the manufacturer's proprietary software. All reconstructed image stacks were brought into standardized anatomical orientation using Dataviewer (Bruker) and converted to NIfTI volumetric format to be loaded into 3D Slicer to visualize the skull morphology. Skull measurements were also taken using 3D Slicer.[33] Soft tissue, such as brain, cannot be effectively imaged via micro-CT. Instead, we chose to look at the endocranial volume, which is tightly correlated with brain size. Although segmenting the endocranial space using automated watershed algorithms from the skull is straightforward, it requires all cranial openings to be sealed digitally, so that segmentation does not leak into other regions. To reduce the amount of manual segmentation and avoid rater bias on measurements, we chose to construct an unbiased atlas of our study population, segment the endocranial space, and warp it back to the constituent samples using deformable registration. We used the open-source DRAMMS deformable registration software and atlas-building pipeline in this study.[34,35] The DRAMMS registration software consists of two major components: attribute matching and mutual-saliency weighting. Attribute matching characterizes each voxel by a high dimensional vector of multi-scale and multi-orientation Ga-

bor attributes. This method provides more information than the intensity information traditionally used (see Developmental Brain ADC Atlas in Web Resources).[34–37] Because the reliability and accessibly of correspondence varies across anatomical structures, mutual-saliency upweights regions of the volume where correspondence can be reliably established between the source and target images. The preferred use of reliable correspondence reduces the negative impact of outlier regions on the registration quality (see Developmental Brain ADC Atlas in Web Resources).[34–37] Atlas construction was performed using the DRAMMS deformable registration in a classic unbiased population registration framework.[37] The atlas construction framework iteratively finds a virtual space that resides in the centroid of the study population (centroid meaning that the deformations needed to transform all subjects into this virtual space sum up to zero everywhere in this virtual space). Therefore, the constructed atlas is unbiased to any subject in the population and is hence representative of the mean anatomy/geometry of the population (see Developmental Brain ADC Atlas in Web Resources).[37] The constructed atlas was segmented using the editor module of 3D Slicer. This reference segmentation was then mapped onto the individual samples by inversing their transformation into the atlas (Figure S7). Individual volumes of endocranial space were calculated after this transformation and are reported in Table S2.

cDNA Cloning and Mutagenesis

Full-length human *CRADD* coding cDNA (GenBank: NM_003805.3) and the coding sequence for the PIDD death domain (PIDD-DD) (*PIDD1* [GenBank: NM_145886.3]) were amplified by PCR from cDNA reverse transcribed from human ARPE-19 cell mRNA using Moloney Murine Leukemia Virus (M-MuLV) reverse transcriptase (NEB). PCR products were ligated into pENTR/D-TOPO (ThermoFisher), and *CRADD* TLIS mutations (c.382G>C, c.491T>G, c.508C>T, c.509G>A) were introduced with site-directed mutagenesis (QuikChange II, Agilent Technologies). LR recombination (LR Clonase II, ThermoFisher) was used to generate FLAG (pCAGIG/RFC-A/N-FLAG) or V5 (pcDNA3.1/N-V5) mammalian expression plasmids from pENTR clones. All clones were verified with Sanger sequencing.

Transduction of Pen1-CRADD

CRADD cDNAs—WT and *CRADD* TLIS variants described above—were subcloned into the Novagen pET15b expression system in-frame with an N/C-terminal polyhistidine sequence downstream of the T7 promoter and expressed in BL21 cells that express the T7 RNA polymerase under an IPTG-inducible promoter. The expressed proteins were purified on a Ni^{2+} resin as previously described.[38] Penetratin 1 (Pen1) was mixed at a 2:1 molar ratio with purified CRADD and incubated 2 hr at 37°C to generate disulfide-linked Pen1-CRADD. Linkage was assessed by 20% SDS-PAGE and by western blotting with anti-His antibody and anti-CRADD antibody as previously described.[39] To ensure uniform protein transduction across cultures, Pen1-CRADD was used at the same concentration (27 nM). PC12 cells and mouse sympathetic neurons take up Pen1 proteins with near 100% efficiency. This approach is more efficient, less cytotoxic, and easier to titrate than transient transfection of cDNA constructs.[40,41]

Cell Lines and Transfection

ARPE-19, HEK293T, and Neuro2a cells used in this study were purchased from the American Type Culture Collection (ATCC).

ARPE-19 cells were cultured in DMEM:F12 with 10% fetal bovine serum (FBS), and HEK293T and Neuro2a were cultured in DMEM with 10% FBS. Cells were transfected with FuGENE 6 (Roche) at a 3:1 FuGENE6:DNA ratio according to the manufacturer's instructions. Primary cultures of dermal fibroblasts from skin biopsies from CRADD TLIS-affected individuals (homozygous c.382G>C [p.Gly128Arg]) and their heterozygous parents were established by the Coriell Institute, and normal human dermal fibroblasts were acquired from Coriell. Fibroblasts were cultured at low passage (≤ 10) in DMEM with 10% FBS. Unless otherwise noted, all cells were maintained at $37°C$ and 5% CO_2. To assess CRADD abundance in subject fibroblasts, cells were lysed in RIPA buffer (50 mM NaCl, 1.0% IGEPAL CA-630, 0.5% sodium deoxycholate, 0.1% SDS, 50 mM Tris [pH 8.0] [Sigma]) containing protease inhibitor cocktail (Roche), phosphatase inhibitor (PhosSTOP, Roche), and 1 mM phenylmethylsulfonyl fluoride (PMSF) for 15 min at $4°C$. Total protein concentration was normalized across affected subject, heterozygous parents, and normal fibroblast samples using the Bradford assay (Bio-Rad), and equal protein loading for immunoblotting was confirmed with mouse monoclonal anti-β-actin labeling (Sigma, 1:1,000,000). CRADD abundance was assessed with rabbit monoclonal anti-human RAIDD antibodies (Abcam cat# ab52621 and ab76465, RRID: AB_882269 and AB_1524296; 1:1,000). Goat anti-mouse IgG-HRP (Cell Signaling, 1:1,500) and goat anti-rabbit IgG-HRP (Cell Signaling, 1:1,500) were used as secondary antibodies. Blots were imaged with enhanced chemiluminescence using SignalFire Plus (Cell Signaling).

PC12 Cell Culture and Viability

PC12 cells obtained from the ATCC were grown as described previously[21] at 7.5% CO_2 on rat-tail collagen-coated dishes in RPMI 1640 medium (Life Sciences) containing 1% penicillin/streptomycin (P/S), 5% fetal calf serum (FCS), and 10% heat-inactivated horse serum (HS, complete medium). PC12 cell survival was scored as reported previously.[42] Culture medium was removed by aspiration and 100 μL of detergent-containing lysis solution was added to the well. This solution dissolves cell membranes, providing a suspension of intact nuclei that were quantified using a hemocytometer. Triplicate wells were scored and values reported as mean ± SEM. Significance was calculated by Student's t test.

Primary Sympathetic Neuron Culture and Viability

Neurons were cultured as described previously.[22,43] In brief, sympathetic neurons were dissected from 1-day-old WT and CRADD-null[17] ($Cradd^{-/-}$) mouse pups. Cultures were maintained in RPMI 1640 medium supplemented with 10% horse serum and mouse nerve growth factor (NGF; 100 ng/ml) on collagen-coated 24-well dishes. At 1 day after plating, uridine (10 μM) and 5-fluorodeoxyuridine (10 μM) were added for 3 days to eliminate non-neuronal cells. Experiments were conducted after 6 days of culture. Viability was determined as previously reported.[22] Each culture was scored as numbers of living phase-bright neurons counted in the same field at various times. Three replicate cultures were assessed for each condition; data were normalized to the number of neurons present in each culture at the time of Pen1-CRADD treatment and are reported as means ± SEM.

Immunofluorescence Microscopy

Cells cultured on uncoated German glass coverslips transfected with pCAG/FLAG-CRADD WT or CRADD-TLIS variant cDNAs were rinsed with PBS at $37°C$ and fixed with 4% paraformaldehyde at $21°C$ for 15 min. Cells were then prepared for immunofluorescence microscopy and documented as described previously.[44] The primary and secondary antibodies used were anti-FLAG M2 (Sigma, 1:1,000) and Alexa Fluor 488-goat anti-mouse IgG$_1$ (ThermoFisher, 1:400), respectively. Nuclei were stained with 1 μg/mL DAPI (Santa Cruz Biotechnology), and coverslips were mounted with Fluoromount-G (Electron Microscopy Sciences).

CRADD and PIDD Co-immunoprecipitation

Co-immunoprecipitation was performed as described previously.[44,45] In brief, pCAG/FLAG-CRADD WT and CRADD-TLIS variant cDNAs or empty vector were co-transfected with pcDNA3.1/V5-PIDD1-DD cDNA in Neuro2a and HEK293T cells for 40–48 hr, after which whole-cell lysates were clarified by centrifugation at 14,000 rpm for 15 min and incubated with anti-FLAG M2 affinity resin (Sigma) for 2 hr with end-over-end mixing at $4°C$. Resin beads were pelleted and washed 3× in Tris-buffered saline (pH 7.2) with protease inhibitor cocktail (Roche), phosphatase inhibitor (PhosSTOP, Roche), 1 mM PMSF, and 0.5%–1% Tween-20, before elution with 150 ng/μL 3x-FLAG peptide (Sigma). Input lysates and eluates were denatured in sample buffer at $100°C$ for 10 min and then immunoblotted with anti-FLAG (Sigma, 1:1,000) and anti-V5 (ThermoFisher, 1:5,000) antibodies.

Caspase-2 and CRADD Co-immunoprecipitation

Mouse IgG or rabbit IgG magnetic beads (Invitrogen) were pre-coated with affinity-purified anti-caspase-2 antibody[42] for 2 hr at $4°C$ on a rotator. In total, 10 μL of anti-caspase-2 antibody was used per 30 μL of beads. PC12 cells were transduced with Pen1-CRADD for 5 hr. Cell lysates were prepared using CHAPS lysis buffer (150 mM KCl, 50 mM HEPES, 0.1% CHAPS, and protease inhibitor cocktail [pH 7.4]).[22] Lysates (70–120 μg) were loaded onto anti-caspase-2 antibody pre-coated beads and incubated overnight at $4°C$ on a rotator. After overnight incubation, the captured proteins were boiled off the beads at $100°C$ for 5 min. The immunoprecipitated samples, along with inputs, were then subjected to western blot analysis using an anti-CRADD antibody (Abnova), an anti-caspase-2 antibody (Alexis), or an anti-ERK antibody (Santa Cruz Biotechnology). Proteins were detected using the Odyssey Infrared Imaging System (LI-COR Biosciences).

Caspase-2 Activity Assay

We adapted an unbiased caspase-2 activity measurement from Jean et al.[43] bVAD-fmk (biotin-Val-Ala-DL-Asp-fluoromethylketone; 50 μM, MP Biomedicals), a biotinylated pan-caspase inhibitor that traps active caspases, was added to PC12 cultures 1 hr prior to treatment with Pen1-CRADD. Cells were lysed in CHAPS buffer. Active caspase-bVAD-fmk complexes were pulled out with streptavidin-coated beads (Invitrogen). Active caspase-2 was detected by western blotting using affinity-purified polyclonal anti-caspase-2 antibody.[42]

Results

Clinical Presentation and Molecular Genetic Analysis of CRADD-Associated Lissencephaly

Review of brain neuroimaging from more than 1,400 subjects with lissencephaly revealed a relatively mild lissencephaly variant characterized by megalencephaly,
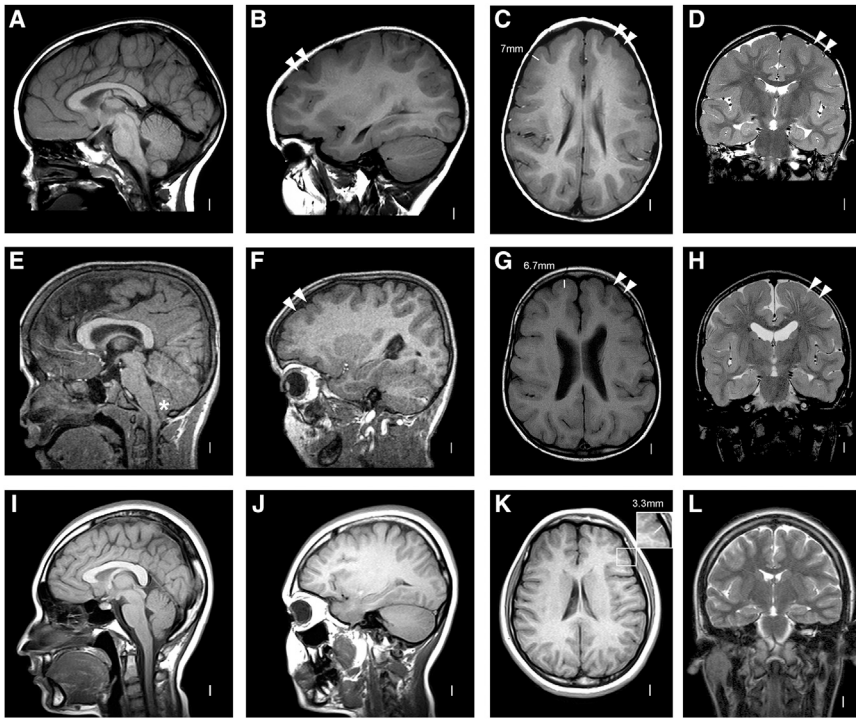
Figure 1. Brain Imaging of TLIS-Affected Individuals with *CRADD* Mutations

(A–D) MRI in subject LR04-101a1 at 5 years shows normal brainstem and cerebellum (A, B), frontal predominant symmetric pachygyria with reduced number of gyri, shallow sulci, and mildly thickened cortex (double arrowheads in B, C, and D with arrowheads located only in the left hemisphere).

(E–H) MRI in subject LR05-279a2 at 7 years demonstrates the same pattern as in the top row (double arrowheads in F, G, and H). The enlargement in the inferior cerebellum is a mild Chiari malformation type I (asterisk in E).

(I–L) Age-matched normal control images. The cortex in TLIS-affected individuals is mildly thick, measuring 5–7 mm in the frontal lobes (see C and G) compared to normal cortex, measuring 3–4 mm (inset in K).

MRI image section planes: A, B, E, F, I, J, sagittal T1-weighted images; C, G, K, axial T1-weighted images; D, H, L, coronal T2-weighted images.

anterior-predominant pachygyria with shallow and unusually wide sulci, mildly thick cortex (5–7 mm) especially in the frontal regions (TLIS), and no non-cortical malformations in 13 families (Figures 1, S1, and S2). Pedigree analysis suggested autosomal-recessive inheritance. Trio-based whole-exome sequencing (WES) in two families with TLIS detected a homozygous mutation of *CRADD* (GenBank: NM_003805.3; c.382G>C [p.Gly128Arg]) in two siblings from a Mennonite family that segregated in the parents.

To identify additional mutations, we performed Sanger sequencing of the two coding exons of *CRADD* in another 18 subjects with TLIS and detected homozygous missense mutations in two affected siblings born to consanguineous Turkish parents (c.508C>T [p.Arg170Cys]) and a proband with Finnish ancestry (c.509G>A [p.Arg170His]), as well as a single variant (c.491T>G [p.Phe164Cys]) in an American boy of Western European background (Table 1). Notably, we previously detected a 3.07 Mb deletion of chromosome 12q22 (chr12: 92,443,579–95,515,465; hg38) in this boy that includes the remaining *CRADD* allele.[46] Targeted panel sequencing in another 148 LIS-affected subjects for whom molecular genetic testing did not detect mutations in any of the known LIS-associated genes did not reveal additional *CRADD* mutations.

The four *CRADD* mutations identified in six individuals from four unrelated families with different ethnic backgrounds are all rare variants (ExAC allele frequency < 0.0005) with high pathogenicity scores (Table 1) that alter highly conserved residues within the CRADD death domain (Figure 2A). The first *CRADD* mutation (c.382G>C [p.Gly128Arg]) that we identified was previously reported in another large family with multiple members presenting with mild to moderate ID;[44] both families belong to the Mennonite (Plain) population of Pennsylvania. The prior family was added to the study, and brain MRI performed in three of seven affected individuals revealed TLIS with normal cerebellum, in line with the MRI features in all other CRADD-TLIS-affected subjects.

Brain imaging and additional clinical data for all affected individuals are shown in Figures 1 and S2 and summarized in Table S1 and Figure S1. Case reports are provided in the Supplemental Data. Of 13 CRADD-TLIS-affected subjects, 9 (69%) had mild intellectual disability (ID), while three had mild to moderate ID and one had borderline ID (IQ = 70–75). Seizures (3 of 13) and additional abnormalities such as hydrocephalus due to Chiari malformation (MIM: 118420) were associated with lower cognitive function. None of the CRADD-TLIS-affected subjects had congenital anomalies other than TLIS, and all were in good general health. Clinical course of the TLIS-affected subjects without *CRADD* mutations was similar to the CRADD-associated group. However, all TLIS-affected individuals without *CRADD* mutations had either normal or small head size. In summary, individuals with recessive *CRADD* mutations (n = 13) presented with TLIS, mild to moderate ID, epilepsy (3 of 13), and either enlarged head size with occipitofrontal circumference (OFC) 2–3 SD (mild megalencephaly in 9 of 13) or true megalencephaly with OFC > 3 SD (2 of 13). One individual had relative megalencephaly, and 1 of the 13 TLIS-affected individuals studied did not have megalencephaly (Table S1).

Table 1. Genotypes of Individuals with *CRADD*-Associated Lissencephaly TLIS

ID	Sex	Ethnic Origin	Genomic Position (hg19)	Affected Transcript HGVS Format (NM_003805.3)	Affected Protein HGVS Format	ExAC Frequency[a]	Frequency in the Population of Origin[a]	PolyPhen-2 Score	SIFT	Mutation Taster	CADD	PhyloP	dbSNP
LR04-101	2 x F	Mennonite	chr12: g.[94243829G>C];[382G>C]	c.[382G>C];[382G>C]	p.[Gly128Arg];[Gly128Arg]	0.000008	0.0172	1.0	tolerated	disease causing	28.3	8,466	rs387906861
LR05-279	F, M	Turkish	chr12: g.[94243955C>T];[508C>T]	c.[508C>T];[508C>T]	p.[Arg170Cys];[Arg170Cys]	0.0000083	n.e.	0.031	damaging	disease causing	24.8	1,654	NA
LR00-150	F	Finnish	chr12: g.[94243956G>A];[509G>A]	c.[509G>A];[509G>A]	p.[Arg170His];[Arg170His]	0.0005277	0.006665	0.995	damaging	disease causing	26.2	2,179	rs141179774
LR02-006	M	Western European	chr12: g.[94243938T>G]	c.[491T>G]	p.Phe164Cys	0.00002496	n.e.	1.0	damaging	disease causing	23.2	6,910	rs37091968
			arr[hg19]12q22(92,837,355–95,909,241x1)	NA	NA	NA	NA	NA	NA	NA	NA	NA	NA

Abbreviations are as follows: TLIS, "thin" lissencephaly; hg19, Genome Reference Consortium Human Build 37 (GRCh37); HGVS, Human Genome Variation Society; ExAC, Exome Aggregation Consortium; CADD, Combined Annotation Dependent Depletion; F, female; M, male; NA, not applicable; n.e., not estimated.
[a]None of the variants were observed homozygously.

TLIS Variants Cluster in the CRADD Death Domain

In response to intrinsic death signals (e.g., genotoxic stress or neurotrophic factor withdrawal), the C-terminal CRADD-DD interacts with the PIDD-DD to form the PIDDosome enabling the N-terminal CRADD CARD domain to interact with and activate caspase-2.[17,18] TLIS-associated CRADD variants (p.Gly128Arg, p.Phe164Cys, p.Arg170Cys, and p.Arg170His) cluster in the DD (Figure 2A), suggesting that they may disrupt interaction with the PIDD-DD.

TLIS CRADD Variants Do Not Disrupt Binding with PIDD or Caspase-2

To determine the functional impact of the TLIS-*CRADD* death domain mutations, we first investigated binding of the CRADD variants to PIDD and caspase-2 and then assessed their ability to induce apoptosis by activating caspase-2. Ultimately, these experiments showed that TLIS-CRADD variants fail to drive caspase-2-initiated apoptosis without significant loss of binding to either PIDD or caspase-2.

In human cells, exogenously expressed p.Gly128Arg CRADD is present at very low abundance, indicating decreased protein stability relative to wild-type (WT) CRADD (Figure 2B). Additionally, it forms abnormal cytosolic clusters (Figure S3) and fails to interact with PIDD in vitro[18,44] (Figure 2D). Dermal fibroblasts from p.Gly128Arg CRADD TLIS-affected subjects are essentially null for CRADD abundance (Figure 2C) relative to heterozygous parent and normal human dermal fibroblasts. Fibroblasts were not available from other CRADD TLIS-affected individuals. However, recombinant p.Phe164Cys, p.Arg170Cys, and p.Arg170His CRADD overexpressed in human cells (ARPE-19, HEK293T) and mouse neuroblasts (Neuro2a) displayed protein abundance and cellular localization comparable to that observed for WT CRADD (Figures 2B and S3), suggesting that the reduced protein abundance observed for p.Gly128Arg CRADD is not a primary pathogenic mechanism in TLIS.

Because the TLIS-*CRADD* mutations cluster in the DD (Figure 2A) where CRADD and PIDD interact,[18] we investigated whether the CRADD variants disrupted interaction with PIDD (PIDD-DD) as we observed for p.Gly128Arg CRADD.[44] Immunoprecipitation of recombinant FLAG-CRADD overexpressed in Neuro2a (data not shown) and HEK293T cells co-precipitated V5-PIDD-DD for each of the CRADD-TLIS variants except p.Gly128Arg (Figure 2D). These data suggest a pathophysiological mechanism other than disrupted PIDD interaction, consistent with our protein structural modeling (see Figure S4 and Discussion) and with the earlier finding that neuronal caspase-2 activation requires CRADD expression but can occur independent of PIDD expression.[22]

Upon activation, the N-terminal caspase-recruitment domain (CARD) of CRADD (Figure 2A) binds with caspase-2 to induce caspase-2 activity.[15,16] To determine whether CRADD-TLIS variants can activate caspase-2, we first determined whether they could bind to caspase-2. To
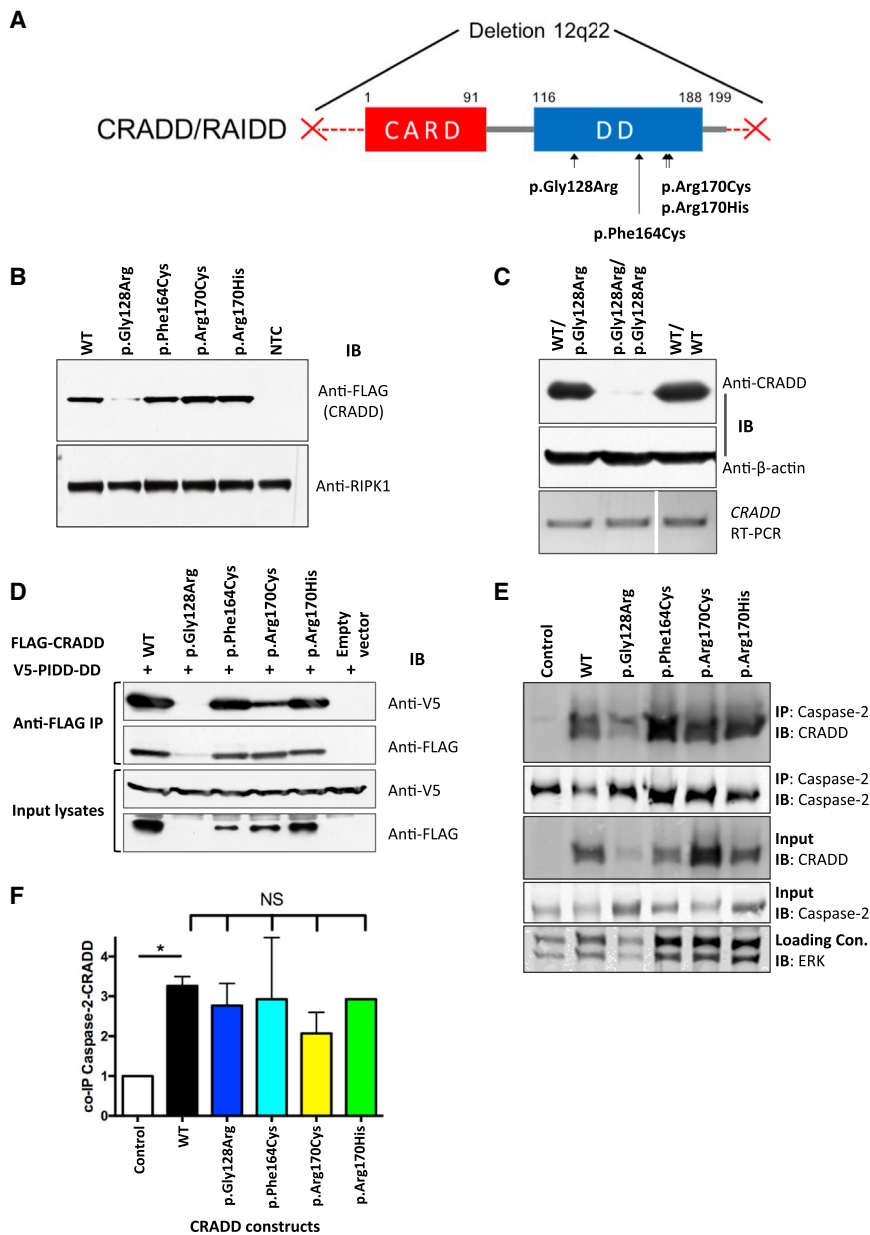
Figure 2. TLIS CRADD Variants Do Not Disrupt Binding with PIDD or Caspase-2

(A) Functional domain structure of CRADD showing TLIS substitutions clustered in the C-terminal death domain (DD, amino acids 116–188). CARD, N-terminal caspase-recruitment domain (amino acids 1–91). CRADD substitutions p.Gly128Arg, p.Arg170Cys, and p.Arg170His are homozygous in individuals with TLIS. The p.Phe164Cys encoding *CRADD* allele (c.491T>G) is in *trans* with a 3.07 Mb deletion of chromosome 12q22 (denoted by the two red Xs) in one TLIS-affected subject (see Table 1).

(B) Immunoblot (IB) of recombinant FLAG-CRADD TLIS variants overexpressed in HEK293T cells (n = 6). NTC, non-transfected control. Receptor-interacting serine/threonine-protein kinase 1 (RIPK1 [MIM: 603453]; 78 kDa) immunoblotting was used as a loading control.

(C) Top: western blot of CRADD (23 kDa) from dermal fibroblasts of a TLIS-affected subject homozygous for p.Gly128Arg CRADD (p.Gly128Arg/p.Gly128Arg) versus heterozygous parent (WT/p.Gly128Arg) and normal human dermal fibroblasts (WT/WT) (n = 4). Anti-β-actin (42 kDa) immunoblotting was used as a loading control. Bottom: Reverse transcriptase-PCR of the full-length human *CRADD* coding sequence (GenBank: NM_003805.3; 658 bp) from CRADD p.Gly128Arg (c.382G>C) TLIS-affected subject dermal fibroblasts (p.Gly128Arg/p.Gly128Arg) versus heterozygous parent (WT/p.Gly128Arg) and normal fibroblasts (WT/WT) demonstrating stability of the mutant transcript. Note: the WT/WT lane of the RT-PCR gel was cropped from the same gel used for the subject and heterozygous parent samples. Cropping is denoted by the white bar separating lanes 2 and 3.

(D) FLAG-CRADD WT and TLIS variants were co-overexpressed with V5-PIDD-DD in HEK293T cells (as indicated) for 40 hr after which FLAG-CRADD was immunoprecipitated (IP) from whole cell lysates (input) with anti-FLAG M2 affinity resin. Co-precip-

itated complexes were first immunoblotted (IB) with anti-V5 antibody (PIDD-DD). Blots were then stripped and reprobed with anti-FLAG antibody (CRADD). CRADD WT and each of the TLIS CRADD variants except for p.Gly128Arg CRADD co-precipitated PIDD-DD (n = 3).
(E and F) Immunoprecipitation (IP) of caspase-2 from PC12 cells 5 hr after the cells were transduced with 27 nM Pen1-CRADD proteins as indicated (n = 2–3). Caspase-2 co-precipitated Pen1-CRADD WT and TLIS variants in similar abundances when corrected for Pen1-CRADD abundance in whole cell lysates (input) as shown in (F). Blots were stripped and reprobed with anti-caspase-2. Error bars represent SEM. NS, no significant difference; control, non-transduced cells. ERK immunoblotting was used as an input lysate loading control. CRADD p.Gly128Arg abundance is always lower in transduced PC12 cells, in agreement with our previous findings.[44]

efficiently deliver CRADD-TLIS variant proteins into cells without the cytotoxic side effects of transient transfection, CRADD-TLIS protein variants were directly linked to Penetratin-1 (Pen1) by a disulfide bond. Pen1 facilitates high-efficiency cellular uptake of linked proteins, and the reducing environment of the cytosol then cleaves the disulfide linkage releasing the transported protein.[40,41] PC12 cells were transduced with Pen1-linked constructs of each of the CRADD-TLIS variants and caspase-2 was immunoprecipitated from whole-cell lysates 5 hr

after transduction. Immunoprecipitated caspase-2 pulled down each of the CRADD-TLIS variants, suggesting that all of the CRADD-TLIS variants can interact with caspase-2 when the blots are normalized for CRADD abundance (Figures 2E and 2F).

TLIS Variants Disrupt CRADD's Ability to Drive Neuronal Apoptosis

One parsimonious explanation for TLIS could be that loss of CRADD function results in reduction of
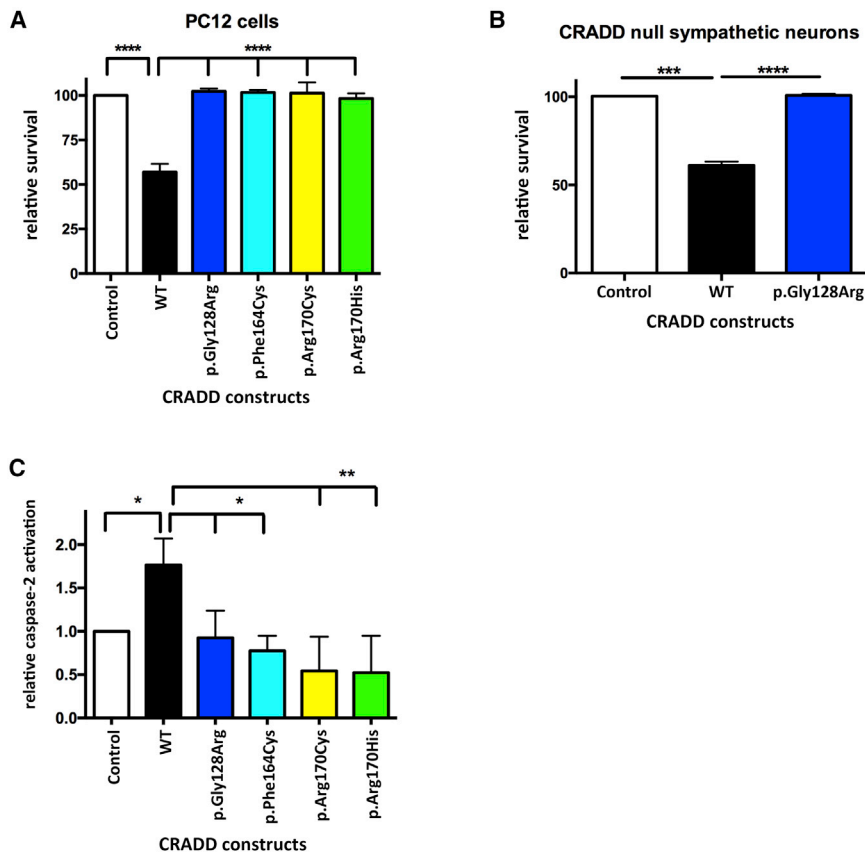
A PC12 cells

B CRADD null sympathetic neurons

C

Figure 3. TLIS-CRADD Variants Fail to Activate Caspase-2-Initiated Apoptosis

(A and B) Pen1-CRADD WT (27 nM) drives apoptosis 1 day after transduction in PC12 cells (A) and in primary sympathetic neurons from $Cradd^{-/-}$ mice (B) whereas Pen1-TLIS-CRADD variants (27 nM) do not (n = 4 for each cell type). Control indicates non-transduced cells.

(C) TLIS-CRADD variants fail to activate caspase-2. PC12 cells were treated with 50 μM bVAD-fmk for 1 hr followed by transduction with 27 nM Pen1-CRADD as indicated for 2 hr. Caspase-bVAD-fmk complexes in whole-cell lysates were precipitated with streptavidin and immunoblotted for caspase-2. Precipitated caspase-2 band optical density was used as a measure of relative caspase-2 activity[42,43] (n = 3). Error bars represent SEM. Control indicates non-transduced cells.

ligand biotin-Val-Ala-DL-Asp-fluoromethylketone (bVAD-fmk), a pan-caspase substrate/inhibitor that binds to the first active caspase, and which we previously showed is effective in measuring caspase-2 activity in PC12 cells.[42,43] PC12 cells were treated with bVAD-fmk for 1 hr prior to transduction with Pen1-CRADD WT and TLIS variants. Two hours after transduction, cells were harvested for streptavidin pulldown of bVAD-fmk:caspase complexes followed by western blotting for caspase-2 (Figure 3C). We found that only WT CRADD induces caspase-2 activity; the CRADD-TLIS variants do not. This suggests that although the CRADD-TLIS variants can bind caspase-2, they are unable to activate caspase-2 and induce apoptosis. In sum, in vitro experiments demonstrated functional defects in caspase-2 activation despite no consistent defects in protein interactions with PIDD or caspase-2.

Cradd Knockout Mice Display Megalencephaly and Seizures Consistent with TLIS

To determine whether loss of CRADD function results in a TLIS-like phenotype in mice, we analyzed cortical morphology and head size in $Cradd^{-/-}$ mice. The $Cradd^{-/-}$ mice used were previously reported to have normal development, although brain morphology and head size were not studied.[17] Volumetric micro-CT skull analysis of $Cradd^{-/-}$ mice relative to heterozygous ($Cradd^{+/-}$) and WT controls demonstrated that all mutant mice had a statistically significant increase in endocast volume that corresponds to increased brain volume (Figure 4). Morphological analysis of $Cradd^{-/-}$ cortex revealed normal layering indistinguishable from WT mice (Figure S5). Notably, 8 of 31 (26%) $Cradd^{-/-}$ mice displayed handling-induced seizures; no WT or $Cradd^{+/-}$ littermates (0 of 60) had seizures.
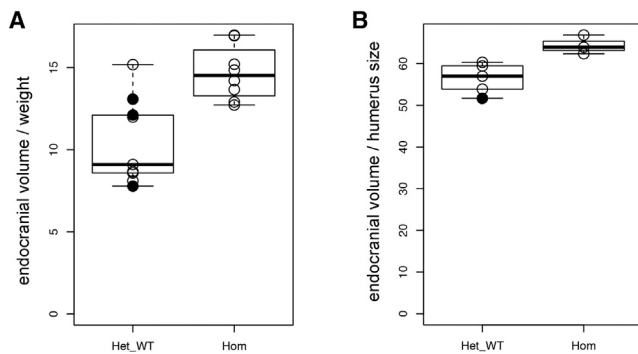
caspase-2-mediated apoptosis, resulting in megalencephaly and TLIS from failure to prune inappropriate neurons and/or neuropil. Overexpression of WT CRADD in PC12 and other mammalian cells (e.g., HEK293) is sufficient to activate caspase-2 and promote apoptosis.[15,47] To examine whether CRADD-TLIS variants fail to induce apoptosis, PC12 cells were transduced with Pen1-linked human WT and CRADD-TLIS variants and cell survival was measured 1 day after treatment. Only WT CRADD import induced apoptosis in PC12 cells. Transduction of PC12 cells with Pen1-linked CRADD-TLIS variants (p.Gly128Arg, p.Phe164Cys, p.Arg170Cys, and p.Arg170His) failed to induce cell death (Figure 3A). To confirm this finding in neurons lacking endogenous CRADD, primary sympathetic neurons from *Cradd* knockout ($Cradd^{-/-}$) mice were transduced with Pen1-linked human WT and p.Gly128Arg CRADD. CRADD WT resulted in significant cell death of primary sympathetic neurons from $Cradd^{-/-}$ mice 1 day after transduction, whereas cell survival after transduction of p.Gly128Arg CRADD was indistinguishable from that of non-transduced cells (Figure 3B).

CRADD TLIS Variants Do Not Activate Caspase-2

All CRADD-TLIS variants bind to caspase-2 but only WT CRADD induces cell death, so we next determined whether CRADD-TLIS variants can induce caspase-2 activation. To measure caspase-2 activity, we used the caspase-affinity

Figure 4. Megalencephaly in *Cradd*^{−/−} Knockout Mice
(A) Boxplot showing the ratio of endocranial volume to body weight in *Cradd* control (heterozygous and wild-type, Het-WT) (n = 9) and *Cradd*^{−/−} knockout (Hom) (n = 8) mice.
(B) Boxplot demonstrating the ratio of endocranial volume to humerus surface area in *Cradd* control (Het-WT) (n = 5) and *Cradd*^{−/−} (Hom) (n = 3) mice. Wild-type and heterozygous mice are shown with closed and open circles, respectively.

Megalencephaly with normal cortical morphology in *Cradd*^{−/−} mice coupled with loss of function in driving apoptosis through caspase-2 activation in the CRADD-TLIS variants in vitro suggest that the cortical malformation in CRADD-TLIS more likely results from reduced caspase-2-mediated apoptosis during cortical development than a neuronal migration disorder.

Discussion

CRADD/Caspase-2-Driven Apoptosis Is Required for Normal Development of Neocortex

Here, we describe a mild "thin" lissencephaly (TLIS) resulting from loss of CRADD function and reduced caspase-2-initiated neuronal apoptosis. Recent reviews have postulated that decreased apoptosis could underlie some human brain overgrowth disorders (e.g., megalencephaly).[48] However, to date no human cortical malformations associated with decreased apoptosis have been reported. The potential impact of reduced apoptosis during mammalian brain development was previously demonstrated by brain malformations in caspase-3-,[49] caspase-9-,[50,51] and Apaf1-[52] deficient mouse embryos and by increased forebrain size in *EphA7*^{−/−} mice[53] resulting from decreased apoptosis of cortical progenitor cells. In contrast to the pachygyria and mildly thick cortex associated with TLIS in humans, caspase-3 (*Casp3*), caspase-9 (*Casp9*), and Apaf1 (*Apaf1*) knockout mice displayed neural tube closure defects, forebrain protrusions of ectopic masses of cortical tissue that deformed the anterior skull, and widespread increased cell density from decreased apoptosis of progenitor cells throughout the brain including the cortex, cerebellum, and brainstem. Overgrowth of progenitors in these mice is thought to result largely from loss of apoptosis of morphogen-producing cells early in development (e.g., FGF8), altering the spatiotemporal morphogen gradients that regulate progenitor expansion and ensure proper forebrain development.[54] During zebrafish development, excessive activation of CRADD/caspase-2 signaling through persistent phosphomimetic activation of Pidd (*pidd1*) resulted in a severe microcephaly phenotype.[19]

TLIS CRADD Variants Fail to Activate Caspase-2-Initiated Apoptosis without Disrupting Interaction between CRADD and PIDD

The recent published structure of the PIDDosome in solution suggests that the PIDDosome core is composed of a CRADD-DD:PIDD-DD stoichiometry of 5:5 with 1–2 additional loosely associated CRADD-DDs.[55] The solution structure suggests that the amino acids altered by TLIS *CRADD* mutations do not participate in intra- or inter-molecular interactions that are critical to the core structure of the PIDDosome, and as such should not alter caspase-2 activation through disrupted CRADD-DD:PIDD-DD interaction. To explore this further, we generated three protein models including the CRADD-TLIS substitutions using SWISS-MODEL, IRECS, and PyMOL (Figure S4). Based on our models and the published data, CRADD Arg170 forms a hydrogen bond with Glu188 on another CRADD-DD, while the adjacent amino acid Ala169 interacts either with Val189 on another CRADD-DD or Arg862 and Arg864 on a PIDD-DD (Figure S4). The substitution of CRADD Arg170 to Cys or His should inhibit hydrogen bond formation with Glu188. However, others recently determined that the 5:5 CRADD-DD:PIDD-DD PIDDosome core is not disrupted by substitution of CRADD Glu188 with Lys and that Glu188 is solvent accessible in the core PIDDosome molecule in solution. This suggests that Arg170 interaction with Glu188 is not fundamentally important to formation of the PIDDosome.[55] Our models also predicted that Gly128 and Phe164 do not participate in an interaction interface and should therefore have no direct contact with any residues of the PIDD-DD (Figure S4).

Our co-immunoprecipitation data showing that all FLAG-CRADD TLIS variants except for p.Gly128Arg CRADD co-precipitate V5-PIDD-DD at abundances similar to FLAG-CRADD WT support the modeling data which suggest that TLIS-associated pathophysiology does not result from impaired CRADD-DD:PIDD-DD interactions. Previous in vitro mutational analysis suggested that p.Arg170Ala-substituted CRADD exhibited a dominant-negative effect interfering with formation of the PIDDosome core by disrupting the interaction between CRADD and PIDD death domains.[56] However, p.Arg170His and p.Arg170Cys CRADD co-precipitated PIDD-DD at abundances comparable to those co-precipitated by wild-type CRADD in our experiments (Figure 2D). Further, adult CRADD p.Arg170His and p.Arg170Cys heterozygotes had no symptoms suggestive of impaired CRADD function, including no unusual sensitivity to genotoxic stress. This suggests that the recent resolution of the structure of the PIDDosome in solution[55] provides a more physiologically relevant model consistent with our data.

The lack of significant phenotypic differences between TLIS-affected individuals homozygous for p.Gly128Arg CRADD that disrupts interaction with the PIDD-DD versus TLIS-affected individuals with CRADD variants that do not disrupt PIDD-DD binding suggests that activation of caspase-2 may be the only function of the PIDDosome during brain development. Alternatively, formation of the PIDDosome may not be required for neuronal apoptosis during brain development. Amyloid-β-induced, CRADD/caspase-2-initiated neuronal apoptosis persists in rat hippocampal neurons depleted of PIDD and NGF withdrawal induces CRADD/caspase-2 driven death of PIDD-null (Pidd1$^{-/-}$) mouse sympathetic neurons.[22]

The TLIS Phenotype Is Present but Less Pronounced in *Cradd* Knockout Mice

Complete loss of CRADD expression during brain development in *Cradd*$^{-/-}$ mice resulted in megalencephaly (Figure 4) and seizures without obvious changes in cortical thickness or lamination (Figure S5). This is in distinct contrast to the severe malformations of brain development described above for caspase-3-, caspase-9-, and Apaf1-null mice.

Previous work demonstrated that *Casp2*$^{-/-}$ mice have significantly reduced body weight and bone volume.[57] We also observed reduced body weight in *Cradd*$^{-/-}$ mice. Further study showed significantly decreased limb size, indicating that the low weight correlated with small body size (Table S2, Figure S6). The decreased body weight and bone volume in *Casp2*$^{-/-}$ and *Cradd*$^{-/-}$ mice correlates with our functional results, which demonstrate loss of caspase-2 activation in the absence of active CRADD. The head size of *Casp2*$^{-/-}$ mice has not yet been assessed.

CRADD activation of caspase-2 in neurons is required for neurotrophic factor withdrawal-induced apoptosis and for dendritic spine collapse and neuronal apoptosis in response to amyloid-β aggregation,[22,58] suggesting a role for CRADD/caspase-2 signaling in synaptic plasticity and cortical architecture during mammalian brain development. The relative lack of a significant CNS phenotype in early studies of *Casp2*$^{-/-}$ mice and the mild megalencephaly described in this study for *Cradd*$^{-/-}$ mice, in contrast to the lissencephaly variant and ID observed in CRADD-TLIS-affected subjects, suggests that caspase-2 activity may be less important in development of the mouse brain than it is in the human brain.

Other Disorders Caused by Decreased Caspase-Mediated Apoptosis

Caspase-dependent apoptosis is characterized by ordered disruption of the cell without induction of inflammation.[59] Caspase activation can be triggered by extracellular signals (extrinsic pathway regulated by multiple death receptors) or intrinsic stress signals such as DNA damage (intrinsic or mitochondrial pathway).[60] Caspase-dependent apoptosis is involved in several different human diseases including neurodegenerative, cardiovascular, and autoimmune disorders and cancer (reviewed by Favaloro et al.[59]). Autoimmune lymphoproliferative syndrome is a Mendelian disorder caused by impaired caspase-mediated apoptosis (MIM: 601859, 603909, and 607271)[61] associated with mutations in *FAS*,[62] *FASLG*,[63] *CASP10*,[64] and *CASP8*[65] (MIM: 134637, 134638, 601762, and 601763, respectively). Individuals with this syndrome develop chronic lymphoproliferation with lymphadenopathy, hepatosplenomegaly, autoimmunity, and increased rates of malignancy[61] but have normal development and intellectual function.

Conclusions

Our data suggest that CRADD/caspase-2 signaling is required for normal development of the human neocortex and normal cognitive function and that decreased caspase-2-mediated apoptosis during human development can result in cortical malformation. Further investigation is required to delineate the role of CRADD/caspase-2 signaling in homeostatic regulation of cortical development. It is not clear whether the megalencephaly, undulating pachygyria, increased cortical thickness, and intellectual disability characteristic of CRADD-TLIS result from reduced pruning of synaptic connections, decreased programmed cell death of inappropriate neurons, or a combination of the two.

Supplemental Data

Supplemental Data include seven figures and two tables and can be found with this article online at http://dx.doi.org/10.1016/j.ajhg.2016.09.010.

Web Resources

3D Slicer, https://www.slicer.org/
1000 Genomes, http://www.internationalgenome.org/
CADD, http://cadd.gs.washington.edu/
dbSNP, http://www.ncbi.nlm.nih.gov/projects/SNP/
Developmental Brain ADC Atlas Creation from Clinical Images, http://www.nmr.mgh.harvard.edu/~you2/publications/BabyAtlasing_OHBM14.pdf
DRAMMS Image Registration Software, https://www.cbica.upenn.edu/sbia/software/dramms/
ExAC Browser, http://exac.broadinstitute.org/
GenBank, http://www.ncbi.nlm.nih.gov/genbank/
IRECS, http://irecs.bioinf.mpi-inf.mpg.de/
MutationTaster, http://www.mutationtaster.org/
NHLBI Exome Sequencing Project (ESP) Exome Variant Server, http://evs.gs.washington.edu/EVS/
OMIM, http://www.omim.org/
PolyPhen-2, http://genetics.bwh.harvard.edu/pph2/
PyMOL, http://www.pymol.org
RCSB Protein Data Bank, http://www.rcsb.org/pdb/home/home.do
RefSeq, http://www.ncbi.nlm.nih.gov/RefSeq
SIFT, http://sift.bii.a-star.edu.sg/
SWISS-MODEL, http://swissmodel.expasy.org/
UCSC Genome Browser, http://genome.ucsc.edu
UCSC Genome Browser: Downloads, http://hgdownload.cse.ucsc.edu/downloads.html

References

1. Bystron, I., Blakemore, C., and Rakic, P. (2008). Development of the human cerebral cortex: Boulder Committee revisited. Nat. Rev. Neurosci. 9, 110–122.

2. Dekkers, M.P., Nikoletopoulou, V., and Barde, Y.A. (2013). Cell biology in neuroscience: Death of developing neurons: new insights and implications for connectivity. J. Cell Biol. 203, 385–393.

3. Hu, W.F., Chahrour, M.H., and Walsh, C.A. (2014). The diverse genetic landscape of neurodevelopmental disorders. Annu. Rev. Genomics Hum. Genet. 15, 195–213.

4. McIlwain, D.R., Berger, T., and Mak, T.W. (2013). Caspase functions in cell death and disease. Cold Spring Harb. Perspect. Biol. 5, a008656.

5. Rakic, P. (2009). Evolution of the neocortex: a perspective from developmental biology. Nat. Rev. Neurosci. 10, 724–735.

6. Fischl, B., and Dale, A.M. (2000). Measuring the thickness of the human cerebral cortex from magnetic resonance images. Proc. Natl. Acad. Sci. USA 97, 11050–11055.

7. Dobyns, W.B., Reiner, O., Carrozzo, R., and Ledbetter, D.H. (1993). Lissencephaly. A human brain malformation associated with deletion of the LIS1 gene located at chromosome 17p13. JAMA 270, 2838–2842.

8. Kato, M., and Dobyns, W.B. (2003). Lissencephaly and the molecular basis of neuronal migration. Hum. Mol. Genet. 12, R89–R96.

9. Moon, H.M., and Wynshaw-Boris, A. (2013). Cytoskeleton in action: lissencephaly, a neuronal migration disorder. Wiley Interdiscip. Rev. Dev. Biol. 2, 229–245.

10. Jamuar, S.S., and Walsh, C.A. (2015). Genomic variants and variations in malformations of cortical development. Pediatr. Clin. North Am. 62, 571–585.

11. Avela, K., Toiviainen-Salo, S., Karttunen-Lewandowski, P., Kauria, L., Valanne, L., and Salonen-Kajander, R. (2012). Frontotemporal pachygyria-two new patients. Eur. J. Med. Genet. 55, 753–757.

12. Guzel, A., Tatli, M., Bilguvar, K., Diluna, M.L., Bakkaloglu, B., Ozturk, A.K., Bayrakli, F., and Gunel, M. (2007). Apparently novel genetic syndrome of pachygyria, mental retardation, seizure, and arachnoid cysts. Am. J. Med. Genet. A. 143A, 672–677.

13. Phadke, S.R., Girisha, K.M., and Phadke, R.V. (2007). A new autosomal recessive disorder of bilateral frontotemporal pachygyria without microcephaly: report of a case and review of literature. Neurol. India 55, 57–60.

14. Ramirez, D., Lammer, E.J., Johnson, C.B., and Peterson, C.D. (2004). Autosomal recessive frontotemporal pachygyria. Am. J. Med. Genet. A. 124A, 231–238.

15. Ahmad, M., Srinivasula, S.M., Wang, L., Talanian, R.V., Litwack, G., Fernandes-Alnemri, T., and Alnemri, E.S. (1997). CRADD, a novel human apoptotic adaptor molecule for caspase-2, and FasL/tumor necrosis factor receptor-interacting protein RIP. Cancer Res. 57, 615–619.

16. Duan, H., and Dixit, V.M. (1997). RAIDD is a new 'death' adaptor molecule. Nature 385, 86–89.

17. Berube, C., Boucher, L.M., Ma, W., Wakeham, A., Salmena, L., Hakem, R., Yeh, W.C., Mak, T.W., and Benchimol, S. (2005). Apoptosis caused by p53-induced protein with death domain (PIDD) depends on the death adapter protein RAIDD. Proc. Natl. Acad. Sci. USA 102, 14314–14320.

18. Tinel, A., and Tschopp, J. (2004). The PIDDosome, a protein complex implicated in activation of caspase-2 in response to genotoxic stress. Science 304, 843–846.

19. Ando, K., Kernan, J.L., Liu, P.H., Sanda, T., Logette, E., Tschopp, J., Look, A.T., Wang, J., Bouchier-Hayes, L., and Sidi, S. (2012). PIDD death-domain phosphorylation by ATM controls pro-death versus prosurvival PIDDosome signaling. Mol. Cell 47, 681–693.

20. Shearwin-Whyatt, L.M., Harvey, N.L., and Kumar, S. (2000). Subcellular localization and CARD-dependent oligomerization of the death adaptor RAIDD. Cell Death Differ. 7, 155–165.

21. Jabado, O., Wang, Q., Rideout, H.J., Yeasmin, M., Guo, K.X., Vekrellis, K., Papantonis, S., Angelastro, J.M., Troy, C.M., and Stefanis, L. (2004). RAIDD aggregation facilitates apoptotic death of PC12 cells and sympathetic neurons. Cell Death Differ. 11, 618–630.

22. Ribe, E.M., Jean, Y.Y., Goldstein, R.L., Manzl, C., Stefanis, L., Villunger, A., and Troy, C.M. (2012). Neuronal caspase 2 activity and function requires RAIDD, but not PIDD. Biochem. J. 444, 591–599.

23. D'Amelio, M., Cavallucci, V., and Cecconi, F. (2010). Neuronal caspase-3 signaling: not only cell death. Cell Death Differ. 17, 1104–1114.

24. D'Amelio, M., Sheng, M., and Cecconi, F. (2012). Caspase-3 in the central nervous system: beyond apoptosis. Trends Neurosci. 35, 700–709.

25. Bergeron, L., Perez, G.I., Macdonald, G., Shi, L., Sun, Y., Jurisicova, A., Varmuza, S., Latham, K.E., Flaws, J.A., Salter, J.C., et al. (1998). Defects in regulation of apoptosis in caspase-2-deficient mice. Genes Dev. *12*, 1304–1314.

26. Kumar, S., Kinoshita, M., Noda, M., Copeland, N.G., and Jenkins, N.A. (1994). Induction of apoptosis by the mouse Nedd2 gene, which encodes a protein similar to the product of the *Caenorhabditis elegans* cell death gene ced-3 and the mammalian IL-1 beta-converting enzyme. Genes Dev. *8*, 1613–1626.

27. Wang, L., Miura, M., Bergeron, L., Zhu, H., and Yuan, J. (1994). Ich-1, an Ice/ced-3-related gene, encodes both positive and negative regulators of programmed cell death. Cell *78*, 739–750.

28. Carlsson, Y., Schwendimann, L., Vontell, R., Rousset, C.I., Wang, X., Lebon, S., Charriaut-Marlangue, C., Supramaniam, V., Hagberg, H., Gressens, P., and Jacotot, E. (2011). Genetic inhibition of caspase-2 reduces hypoxic-ischemic and excitotoxic neonatal brain injury. Ann. Neurol. *70*, 781–789.

29. Gripp, K.W., Hopkins, E., Doyle, D., and Dobyns, W.B. (2010). High incidence of progressive postnatal cerebellar enlargement in Costello syndrome: brain overgrowth associated with HRAS mutations as the likely cause of structural brain and spinal cord abnormalities. Am. J. Med. Genet. A. *152A*, 1161–1168.

30. Boyle, E.A., O'Roak, B.J., Martin, B.K., Kumar, A., and Shendure, J. (2014). MIPgen: optimized modeling and design of molecular inversion probes for targeted resequencing. Bioinformatics *30*, 2670–2672.

31. Hiatt, J.B., Pritchard, C.C., Salipante, S.J., O'Roak, B.J., and Shendure, J. (2013). Single molecule molecular inversion probes for targeted, high-accuracy detection of low-frequency variation. Genome Res. *23*, 843–854.

32. Gage, G.J., Kipke, D.R., and Shain, W. (2012). Whole animal perfusion fixation for rodents. J. Vis. Exp. *65*, 3564.

33. Fedorov, A., Beichel, R., Kalpathy-Cramer, J., Finet, J., Fillion-Robin, J.C., Pujol, S., Bauer, C., Jennings, D., Fennessy, F., Sonka, M., et al. (2012). 3D Slicer as an image computing platform for the Quantitative Imaging Network. Magn. Reson. Imaging *30*, 1323–1341.

34. Dawant, B.M., Christensen, G.E., Fitzpatrick, J.M., and Rueckert, D., eds. (2012). Biomedical Image Registration, 5th International Workshop, WBIR 2012, Nashville, Tennessee, USA, July 7–8, 2012, Proceedings. In Lecture Notes in Computer Science (New York: Springer).

35. Ou, Y., Sotiras, A., Paragios, N., and Davatzikos, C. (2011). DRAMMS: Deformable registration via attribute matching and mutual-saliency weighting. Med. Image Anal. *15*, 622–639.

36. Doshi, J.J., Erus, G., Ou, Y., and Davatzikos, C. (2013). Ensemble-based medical image labeling via sampling morphological appearance manifolds. Proceedings of MICCAI Challenge Workshop on Segmentation: Algorithms, Theory and Applications, 148–151.

37. Guimond, A., Meunier, J., and Thirion, J.-P. (2000). Average brain models: A convergence study. Comput. Vis. Image Underst. *77*, 192–210.

38. Denault, J.B., and Salvesen, G.S. (2008). Apoptotic caspase activation and activity. Methods Mol. Biol. *414*, 191–220.

39. Akpan, N., Serrano-Saiz, E., Zacharia, B.E., Otten, M.L., Ducruet, A.F., Snipas, S.J., Liu, W., Velloza, J., Cohen, G., Sosunov, S.A., et al. (2011). Intranasal delivery of caspase-9 inhibitor reduces caspase-6-dependent axon/neuron loss and improves neurological function after stroke. J. Neurosci. *31*, 8894–8904.

40. Davidson, T.J., Harel, S., Arboleda, V.A., Prunell, G.F., Shelanski, M.L., Greene, L.A., and Troy, C.M. (2004). Highly efficient small interfering RNA delivery to primary mammalian neurons induces microRNA-like effects before mRNA degradation. J. Neurosci. *24*, 10040–10046.

41. Troy, C.M., Stefanis, L., Prochiantz, A., Greene, L.A., and Shelanski, M.L. (1996). The contrasting roles of ICE family proteases and interleukin-1beta in apoptosis induced by trophic factor withdrawal and by copper/zinc superoxide dismutase down-regulation. Proc. Natl. Acad. Sci. USA *93*, 5635–5640.

42. Troy, C.M., Stefanis, L., Greene, L.A., and Shelanski, M.L. (1997). Nedd2 is required for apoptosis after trophic factor withdrawal, but not superoxide dismutase (SOD1) downregulation, in sympathetic neurons and PC12 cells. J. Neurosci. *17*, 1911–1918.

43. Jean, Y.Y., Ribe, E.M., Pero, M.E., Moskalenko, M., Iqbal, Z., Marks, L.J., Greene, L.A., and Troy, C.M. (2013). Caspase-2 is essential for c-Jun transcriptional activation and Bim induction in neuron death. Biochem. J. *455*, 15–25.

44. Puffenberger, E.G., Jinks, R.N., Sougnez, C., Cibulskis, K., Willert, R.A., Achilly, N.P., Cassidy, R.P., Fiorentini, C.J., Heiken, K.F., Lawrence, J.J., et al. (2012). Genetic mapping and exome sequencing identify variants associated with five novel diseases. PLoS ONE *7*, e28936.

45. Jinks, R.N., Puffenberger, E.G., Baple, E., Harding, B., Crino, P., Fogo, A.B., Wenger, O., Xin, B., Koehler, A.E., McGlincy, M.H., et al. (2015). Recessive nephrocerebellar syndrome on the Galloway-Mowat syndrome spectrum is caused by homozygous protein-truncating mutations of WDR73. Brain *138*, 2173–2190.

46. Sajan, S.A., Fernandez, L., Nieh, S.E., Rider, E., Bukshpun, P., Wakahiro, M., Christian, S.L., Rivière, J.B., Sullivan, C.T., Sudi, J., et al. (2013). Both rare and de novo copy number variants are prevalent in agenesis of the corpus callosum but not in cerebellar hypoplasia or polymicrogyria. PLoS Genet. *9*, e1003823.

47. Wang, Q., Maniati, M., Jabado, O., Pavlaki, M., Troy, C.M., Greene, L.A., and Stefanis, L. (2006). RAIDD is required for apoptosis of PC12 cells and sympathetic neurons induced by trophic factor withdrawal. Cell Death Differ. *13*, 75–83.

48. Mirzaa, G.M., and Poduri, A. (2014). Megalencephaly and hemimegalencephaly: breakthroughs in molecular etiology. Am. J. Med. Genet. C. Semin. Med. Genet. *166C*, 156–172.

49. Kuida, K., Zheng, T.S., Na, S., Kuan, C., Yang, D., Karasuyama, H., Rakic, P., and Flavell, R.A. (1996). Decreased apoptosis in the brain and premature lethality in CPP32-deficient mice. Nature *384*, 368–372.

50. Hakem, R., Hakem, A., Duncan, G.S., Henderson, J.T., Woo, M., Soengas, M.S., Elia, A., de la Pompa, J.L., Kagi, D., Khoo, W., et al. (1998). Differential requirement for caspase 9 in apoptotic pathways in vivo. Cell *94*, 339–352.

51. Kuida, K., Haydar, T.F., Kuan, C.Y., Gu, Y., Taya, C., Karasuyama, H., Su, M.S., Rakic, P., and Flavell, R.A. (1998). Reduced apoptosis and cytochrome c-mediated caspase activation in mice lacking caspase 9. Cell *94*, 325–337.

52. Yoshida, H., Kong, Y.Y., Yoshida, R., Elia, A.J., Hakem, A., Hakem, R., Penninger, J.M., and Mak, T.W. (1998). Apaf1 is required for mitochondrial pathways of apoptosis and brain development. Cell *94*, 739–750.

53. Depaepe, V., Suarez-Gonzalez, N., Dufour, A., Passante, L., Gorski, J.A., Jones, K.R., Ledent, C., and Vanderhaeghen, P. (2005). Ephrin signalling controls brain size by regulating apoptosis of neural progenitors. Nature *435*, 1244–1250.

54. Nonomura, K., Yamaguchi, Y., Hamachi, M., Koike, M., Uchiyama, Y., Nakazato, K., Mochizuki, A., Sakaue-Sawano, A., Miyawaki, A., Yoshida, H., et al. (2013). Local apoptosis modulates early mammalian brain development through the elimination of morphogen-producing cells. Dev. Cell 27, 621–634.

55. Nematollahi, L.A., Garza-Garcia, A., Bechara, C., Esposito, D., Morgner, N., Robinson, C.V., and Driscoll, P.C. (2015). Flexible stoichiometry and asymmetry of the PIDDosome core complex by heteronuclear NMR spectroscopy and mass spectrometry. J. Mol. Biol. 427, 737–752.

56. Jang, T.H., Seo, E.K., and Park, H.H. (2013). Analysis of mutation effects on PIDDosome core complex. Appl. Biochem. Biotechnol. 170, 210–218.

57. Shalini, S., Dorstyn, L., Wilson, C., Puccini, J., Ho, L., and Kumar, S. (2012). Impaired antioxidant defence and accumulation of oxidative stress in caspase-2-deficient mice. Cell Death Differ. 19, 1370–1380.

58. Pozueta, J., Lefort, R., Ribe, E.M., Troy, C.M., Arancio, O., and Shelanski, M. (2013). Caspase-2 is required for dendritic spine and behavioural alterations in J20 APP transgenic mice. Nat. Commun. 4, 1939.

59. Favaloro, B., Allocati, N., Graziano, V., Di Ilio, C., and De Laurenzi, V. (2012). Role of apoptosis in disease. Aging (Albany, N.Y.) 4, 330–349.

60. Troy, C.M., and Jean, Y.Y. (2015). Caspases: therapeutic targets in neurologic disease. Neurotherapeutics 12, 42–48.

61. Teachey, D.T., Seif, A.E., and Grupp, S.A. (2010). Advances in the management and understanding of autoimmune lymphoproliferative syndrome (ALPS). Br. J. Haematol. 148, 205–216.

62. Fisher, G.H., Rosenberg, F.J., Straus, S.E., Dale, J.K., Middleton, L.A., Lin, A.Y., Strober, W., Lenardo, M.J., and Puck, J.M. (1995). Dominant interfering Fas gene mutations impair apoptosis in a human autoimmune lymphoproliferative syndrome. Cell 81, 935–946.

63. Wu, J., Wilson, J., He, J., Xiang, L., Schur, P.H., and Mountz, J.D. (1996). Fas ligand mutation in a patient with systemic lupus erythematosus and lymphoproliferative disease. J. Clin. Invest. 98, 1107–1113.

64. Wang, J., Zheng, L., Lobito, A., Chan, F.K., Dale, J., Sneller, M., Yao, X., Puck, J.M., Straus, S.E., and Lenardo, M.J. (1999). Inherited human Caspase 10 mutations underlie defective lymphocyte and dendritic cell apoptosis in autoimmune lymphoproliferative syndrome type II. Cell 98, 47–58.

65. Chun, H.J., Zheng, L., Ahmad, M., Wang, J., Speirs, C.K., Siegel, R.M., Dale, J.K., Puck, J., Davis, J., Hall, C.G., et al. (2002). Pleiotropic defects in lymphocyte activation caused by caspase-8 mutations lead to human immunodeficiency. Nature 419, 395–399.